Enzymatic Hydrolysis of *p*-Nitroacetanilide: Mechanistic Studies of the Aryl Acylamidase from *Pseudomonas fluorescens*

Ross L. Stein*

Department of Chemical Enzymology, DuPont Pharmaceuticals Company, Wilmington, Delaware 19880

Received September 20, 2001; Revised Manuscript Received November 6, 2001

ABSTRACT: Aryl acylamidase (EC 3.1.5.13; AAA) catalyzes the hydrolysis of *p*-nitroacetanilide (PNAA) via the standard three-step mechanism of serine hydrolases: binding of substrate (K_s), acylation of active-site serine (k_{acyl}), and hydrolytic deacylation (k_{deacyl}). Key mechanistic findings that emerged from this study include that (1) AAA requires a deprotonated base with a pK_a of 8.3 for expression of full activity toward PNAA. Limiting values of kinetic parameters at high pH are $k_c = 7\ s^{-1}$, $K_m = 20\ \mu M$, and $k_c/K_m = 340\ 000\ M^{-1}\ s^{-1}$. (2) At pH 10, where all the isotope effects were conducted, k_c is equally rate-limited by k_{acyl} and k_{deacyl}. (3) The following isotope effects were determined: $^{D_2O}(k_c/K_m) = 1.7 \pm 0.2$, $^{D_2O}k_c = 3.5 \pm 0.3$, and $^{\beta D}(k_c/K_m) = 0.83 \pm 0.04$, $^{\beta D}k_c = 0.96 \pm 0.01$. These values, together with proton inventories for k_c/K_m and k_c, suggest the following mechanism: (i) The initial binding of substrate to enzyme to form the Michaelis complex is accompanied by solvation changes that generate solvent deuterium isotope effects originating from hydrogen ion fractionation at multiple sites on the enzyme surface. (ii) From within the Michaelis complex, the active site serine attacks the carbonyl carbon of PNAA with general-base catalysis to form a substantially tetrahedral transition state enroute to the acyl-enzyme. (iii) Finally, deacylation occurs through a process involving a rate-limiting solvent isotope effect, generating conformational change of the acyl-enzyme that positions the carbonyl bond in a polarizing environment that is optimal for attack by water.

Enzyme catalysis of amide hydrolysis remains an area of keen interest in bioorganic chemistry, in part due to the largely unexplained rate enhancements that are observed for these reactions. Understanding the molecular origins of these rate enhancements, which can approach 10^{13} (*1*), is important from both a fundamental point of view, where this knowledge would inform general theories of enzyme catalysis, as well as from a practical point of view, where this knowledge would impact on inhibitor and catalyst design.

To approach this problem, one would like to undertake detailed investigations of both the enzymatic reaction and its nonenzymatic counterpart. Of course, for most enzyme systems, this is extremely challenging due to the slowness of the nonenzymatic reaction. And this is certainly the case for amides, where the $t_{1/2}$ for hydrolysis at neutral pH has been estimated to be over a century (*1*).

Anilides, on the other hand, hydrolyze orders of magnitude more rapidly than amides and have frequently served as amide surrogates in mechanistic studies. Numerous studies have been reported for the hydrolysis of the prototype anilide, *p*-nitroacetanilide, and support the mechanism of Scheme 1 involving [HO$^-$]-dependent changes in both rate-limiting step and reaction pathway (*2*−*5*). The rate law for this mechanism is given by the expression of eq 1 where $k_2 = (k_1/k_{-1})k_2'$ and $k_3 = (k_1/k_{-1})K_{a,TI}k_3'$.

Scheme 1: Mechanism for the Alkaline Hydrolysis of *p*-Nitroacetanilide

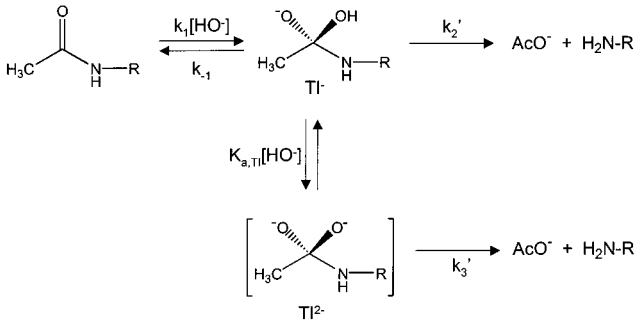

$$k_{obs} = \frac{k_1[HO^-](k_2 + k_3[HO^-])}{k_1 + k_2 + k_3[HO^-]} \quad (1)$$

According to this mechanism, at high [HO$^-$] (>1 M), hydrolysis occurs through the intermediacy of a dianionic tetrahedral intermediate, TI^{2-}, whose rapid decomposition renders hydroxide attack on PNAA via k_1 rate-limiting. As [HO$^-$] is decreased into the range 10^{-2}−10^{-1} M, a complex situation unfolds in which all three reaction steps (i.e., k_1, k_2', and k_3') become partially rate-limiting. Finally, at even lower [HO$^-$] (<10^{-2} M), hydroxide can no longer trap TI$^-$ and decomposition of TI$^-$ occurs exclusively through k_2'. Since breakdown of TI$^-$ to starting materials is generally a

* Current address: Laboratory for Drug Discovery in Neurodegeneration, Harvard Center for Neurodegeneration and Repair, 65 Landsdowne Street, Fourth Floor, Cambridge, MA 02139. Phone: 617-768-8651. Fax: 617-768-8651. E-mail: rstein@rics.bwh.harvard.edu.

10.1021/bi0118198 CCC: $22.00
Published on Web 12/20/2001

Scheme 2: Acylenzyme Mechanism for Serine Hydrolases

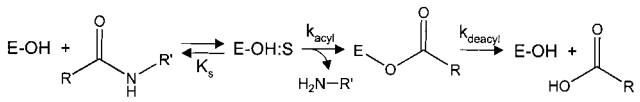

more facile process than is expulsion of aniline from TI^-, k_2' is rate-limiting at low [HO^-] and eq 1 simplifies to $k_{obs} = k_2[HO^-]$.

It is in this low [HO^-] regime where comparison to enzymic reactions becomes appropriate. Much of the mechanistic complexity that accompanies alkaline hydrolysis of PNAA[1] disappears at pH values less than 11, where this reaction proceeds through TI^- with protolytic assistance from solvent of the expulsion of *p*-nitroaniline (*4*, *6*). Additional mechanistic insight has been gained through the determination of β-deuterium isotope effects (*3*, *4*), which suggest that the rate-limiting transition state for the process governed by k_2 has a large degree of tetrahedral character. Since decomposition of TI^- rate-limits the reaction at low pH, this implies an early transition state, relative to the tetrahedral intermediate, for decomposition of TI^- via k_2'.

The detailed mechanistic picture that has emerged for alkaline hydrolysis of PNAA begs comparison to the enzyme-catalyzed hydrolysis of PNAA. While the ultimate concern will be to obtain an understanding of how these enzymes effect catalysis of PNAA hydrolysis, an initial goal must be to provide an understanding of the kinetics and mechanism of one such enzyme. To this end, I have studied and now report on the hydrolysis of PNAA by aryl acylamidases (EC 3.1.5.13) from *Pseudomonas fluorescens*.

Aryl acylamidase from *P. fluorescens* is a 52 kDa monomeric enzyme that catalyzes the hydrolysis of simple alkyl anilides, including PNAA (*7*, *8*). Little is known of the mechanism of this enzyme, other than that its activity increases with increasing pH to a maximum at pH 10 (*8*) and is inactivated by diisopropyl fluorophosphate (*7*). These observations suggest a hydrolytic mechanism involving the nucleophilic participation of an active site serine and probably some form of protolytic catalysis. By analogy to reactions of other serine hydrolases, hydrolysis of PNAA by AAA would proceed through the general mechanism of Scheme 2 involving the intermediacy of an acylenzyme species. This mechanism is described by the steady-state rate expressions of eqs 2−4.

$$\frac{k_c}{K_m} = \frac{k_{acyl}}{K_s} \tag{2}$$

$$k_c = \frac{k_{acyl}k_{deacyl}}{k_{acyl} + k_{deacyl}} \tag{3}$$

$$K_m = K_s\left(\frac{k_{deacyl}}{k_{acyl} + k_{deacyl}}\right) \tag{4}$$

In this study, I report results of experiments that more finely define the catalytic mechanism of AAA-catalyzed hydrolysis of PNAA. Steady-state rate experiments support the general mechanism of Scheme 2 with partial rate-limitation of k_c by k_{deacyl} (i.e., $k_{acyl} \sim k_{deacyl}$). Substrate β-deuterium and solvent deuterium isotope effect experiments were conducted to probe the structure of the rate-limiting transition states for the processes governed by k_c/K_m and k_c and suggest that both are rate-limited by general acid/base-catalyzed chemical transformations of the substrate. Finally, these results are interpreted in the context of transition state rate theory to gain an understanding of the molecular origins of catalysis by this enzyme.

[1] Abbreviations: PNAA, *p*-nitroacetanilide; PNPA, *p*-nitrophenylacetate; AAA, aryl acylamidase.

MATERIALS AND METHODS

General. Buffer salts, *p*-nitrophenylacetate, and deuterium oxide were from Sigma Chemical Co. Buffer solutions for the pH dependencies, solvent isotope effect studies, and proton inventory experiments were prepared as previously describe (*9*). PNAA and d_3–PNAA were purchased from New England Peptides (Fitchburg, MA). Purity was >99% as judged by HPLC analysis and the structure was confirmed by mass spectral analysis (MALDI-TOF DE; within 0.1% of exact molecular weight). Aryl acylamidase from *P. fluorescens* was purchased from BostonBiochem (Cambridge, MA) as a homogeneous protein preparation. The stock solution had a protein concentration of 0.4 mg/mL (7.1 μM) in 50 mM HEPES, 50 mM NaCl, pH 7.6. Aliquots were stored at −20 °C and, when thawed, were stable for at least 1 week if kept at 4 °C.

Kinetic Methods. In a typical kinetic run, 1−10 μL of a solution of PNAA in DMSO was added to 2.00 mL of buffer in a 3 mL cuvette, and the cuvette was placed in the jacketed cell holder of a Perkin-Elmer Lambda 20 spectrophotometer. Reaction temperature was maintained at 25.0 ± 0.1 °C by a circulating water bath. After the reaction solution had reached thermal equilibrium (~5 min), an aliquot of stock AAA was added to the cuvette to initiate the reaction. Reaction progress was monitored by the increase in absorbance at 410 nm (ϵ_{410} = 8800) that accompanies hydrolysis of the *p*-nitroanilide substrate and release of *p*-nitroaniline. For each kinetic, run 100−3000 data points, corresponding to {time, absorbance} pairs, were collected by a PC interfaced to the spectrophotometer.

RESULTS

pH-Dependencies of Steady-State Kinetic Parameters for Aryl Acylamidase Catalysis. Initial velocities were determined as a function of substrate concentration at pH values ranging from 8.0 to 11.0 for the AAA-catalyzed hydrolysis of PNAA. For pH values from 8.0 to 10.0, the buffers were 50 mM Bicine and 500 mM KCl, while at pH 11.0 the buffer was 50 mM $NaCO_3$, 500 mM KCl. Choice of buffer salts and pH range were dictated by two preliminary findings: (1) sulfonate-based buffers, such as HEPES and CAPS, are inhibitory and (2) at pH values below 7.5, independent of buffer salt, reaction velocities are disproportionately depressed.

In these experiments, substrate concentration was varied from 4 to 250 μM. The data at each pH value were fit to the Michaelis−Menten equation to provide the values of k_c and k_c/K_m that are plotted as a function of pH in Figure 1.

The results of Figure 1 indicate that both k_c and k_c/K_m require a deprotonated base for expression of full activity. The pH dependence of both steady-state parameters were

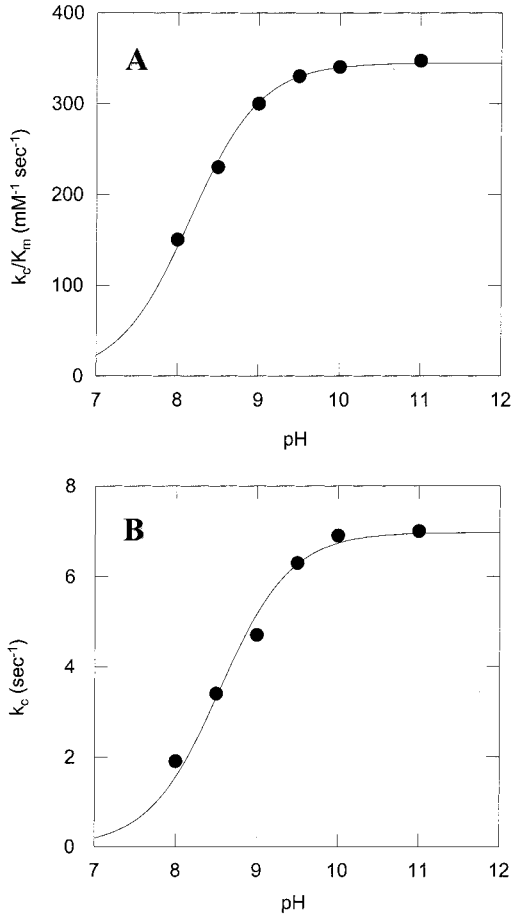

FIGURE 1: pH-dependencies of steady kinetic parameters for the aryl acylamidase-catalyzed hydrolysis of *p*-nitroacetanilide. (Panel A) Dependence of k_c/K_m on pH. Line drawn through the data was according to eq 5 and the best-fit parameters: $(k_c/K_m)_{limit} = 344 \pm 3$ mM^{-1} s^{-1} and p$K_a = 8.15 \pm 0.03$. (Panel B) Dependence of k_c on pH. Line drawn through the data was according to eq 1 and the best-fit parameters: $(k_c)_{limit} = 6.97 \pm 0.20$ s^{-1} and p$K_a = 8.54 \pm 0.06$. See Results section for buffers used, 25 °C. 4 μM ≤ [PNAA] ≤ 250 μM; [AAA] = 7 nM.

Table 1: Solvent Isotope Effects for Aryl Acylamidase Catalysis[a]

			k_{H_2O}/k_{D_2O}	
kinetic parameter	H_2O	D_2O	ratios of rate constants	direct fit to eq 2
k_c (s^{-1})	7.1 ± 0.3	2.1 ± 0.1	3.4	3.5 ± 0.3
k_c/K_m (mM^{-1} s^{-1})	280 ± 11	160 ± 14	1.8	1.7 ± 0.2
K_m (μM)	25 ± 3	13 ± 2	1.9	

[a] Steady-state kinetic parameters were determined from the dependence of steady-state velocity on substrate concentration according to the Michaelis−Menten equation. Error limits for the steady-state kinetic parameters are from the nonlinear fitting procedure. Reaction conditions: 50 mM Bicine, 500 mM KCl, pH 10 and pD equivalent, 25 °C. 4 μM ≤ [PNAA] ≤ 250 μM; [AAA] = 7 nM.

fit to the general equation

$$k_{obs} = \frac{k_{limit}}{1 + 10^{pK_a - pH}} \quad (5)$$

k_c/K_m has a limiting value of 344 ± 3 mM^{-1} s^{-1} and titrates with a pK_a value of 8.15 ± 0.03, while k_c has a limiting value of 7.0 ± 0.2 s^{-1} and titrates with a pK_a value of 8.54 ± 0.06.

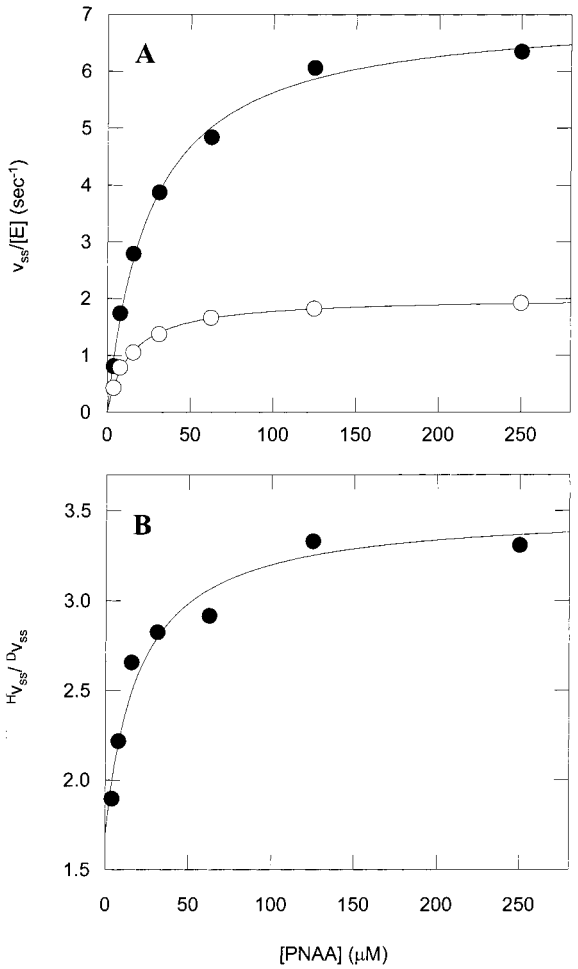

FIGURE 2: Solvent isotope effects for the aryl acylamidase catalyzed hydrolysis of *p*- nitroacetanilide. (Panel A) Solid circles correspond to initial velocities determined in H_2O, while open circles correspond to D_2O. Lines through the points were drawn using the Michaelis−Menten equation and the best-fit parameters summarized in Table 1. (Panel B) Data points are the ratio $^{H}v_{ss}/^{D}v_{ss}$ plotted as a function of substrate concentration. Solid line was drawn using the expression of eq 6 and the best-fit parameters: $^{D_2O}k_c = 3.5 \pm 0.3$, $^{D_2O}(k_c/K_m) = 1.7 \pm 0.2$, $K_m = 20 \pm 4$ μM. Reaction conditions: 50 mM Bicine, 500 mM KCl, pH 10.0 and pD equivalent, 25 °C. 4 μM ≤ [PNAA] ≤ 250 μM; [AAA] = 7 nM.

Solvent Isotope Effects for Catalysis by Aryl Acylamidase. For the AAA-catalyzed hydrolysis of PNAA, values of k_c, K_m, and k_c/K_m were determined in H_2O and D_2O buffers (see Figure 2A). These values together with their ratios (i.e., solvent deuterium isotope effects) are summarized in Table 1.

In Figure 2B, the primary steady-state velocity data is expressed as ratio the $^{H}v_{ss}/^{D}v_{ss}$ and plotted as a function of substrate concentration (*9*). For a simple enzymatic reaction that follows Michaelis−Menten kinetics, the dependence of $^{H}v_{ss}/^{D}v_{ss}$ on $[S]_o$ is given by

$$^{D_2O}v = \frac{^{D_2O}\left(\frac{k_c}{K_m}\right)\left(\frac{K_m}{[S]_o}\right) + {}^{D_2O}k_c}{1 + \frac{K_m}{[S]_o}} \quad (6)$$

The data of Figure 2B were fit to this equation with the following results: $^{D_2O}k_c = 3.5 \pm 0.3$, $^{D_2O}(k_c/K_m) = 1.7 \pm$

0.2, $K_m = 20 \pm 4$ μM. The isotope effects calculated by this method agree with those derived from calculating the ratios of the steady-state parameters, and the value of K_m agrees with independently determined values at this pH. In general, this method of calculating isotope effects for steady-state kinetic parameters provides more accurate values than simply calculating the ratio of independently determined parameters (*9*).

Proton Inventory of Aryl Acylamidase Catalysis. To aid the interpretation of the solvent isotope effect date, we determined the proton inventories for both k_c/K_m and k_c. In proton inventory experiments, a rate constant is determined as a function of mole fraction solvent deuterium, n_{D_2O} (*10*). The shape of this dependence is diagnostic of certain features of the mechanism. In the present case, values of k_c/K_m were determined from pseudo-first-order rate constants determined at low substrate concentration (i.e., $[S]_o = 2.0$ μM $= 0.08K_m$), while values of k_c were determined from steady-state velocities recorded at saturating concentrations of substrate (i.e., $[S]_o = 250$ μM $= 10K_m$). Values of these rate constants were plotted as a function of n_{D_2O} and are shown in Figure 3.

The starting point for the analysis of the proton inventory of Figure 3 is a version of the Gross−Butler equation that is useful in analyzing proton inventories for serine hydrolases (*11, 12*)

$$k_n = k_0 Z^n \frac{\prod(1 - n + n\phi_i^{T})}{\prod(1 - n + n\phi_j^{R})} \quad (7)$$

where k_n is the rate constant at mole fraction solvent deuterium n, k_0 is the rate constant in pure H_2O (i.e., $n = 0$), Z is a solvation term reflecting the composite isotope effect that is generated by small fractionation factors at many protonic sites, and ϕ_i^T and ϕ_j^R are the isotopic fraction factors for the ith and jth proton that is transferred in the transition state and reactant state, respectively. Since reactant state fractionation factors for reactions of serine hydrolases are typically unity (*10*), the Gross−Butler equation can be simplified to

$$k_n = k_0 Z^n \prod(1 - n + n\phi_i^{T}) \quad (8)$$

A final simplification is allowed by the fact that proton inventory data for enzymic reactions are seldom of sufficient precision to allow estimation of the fractionation factors for the individual protonic sites. Thus, values of ϕ_i are assumed to be approximately equal and eq 8 is recast as

$$k_n = k_0 Z^n (1 - n + n\phi^{T})^i \quad (9)$$

In the limit of infinite fractionating protonic sites, eq 8 takes on the form of eq 10

$$k_n = k_0 Z^n (\prod \phi^{T})^n = k_0 Z^n (\Phi^{T})^n \quad (10)$$

where Φ^T is the product of all the individual fractionation factors, ϕ^T, that contribute to the isotope effect (*8*).

The proton inventory data for k_c/K_m (Figure 3A) generates an overall isotope effect of 1.63 that is in good agree with the $^{D_2O}(k_c/K_m)$ value of 1.7 reported above. Examination of this proton inventory reveals that it is slightly "dome-shaped".

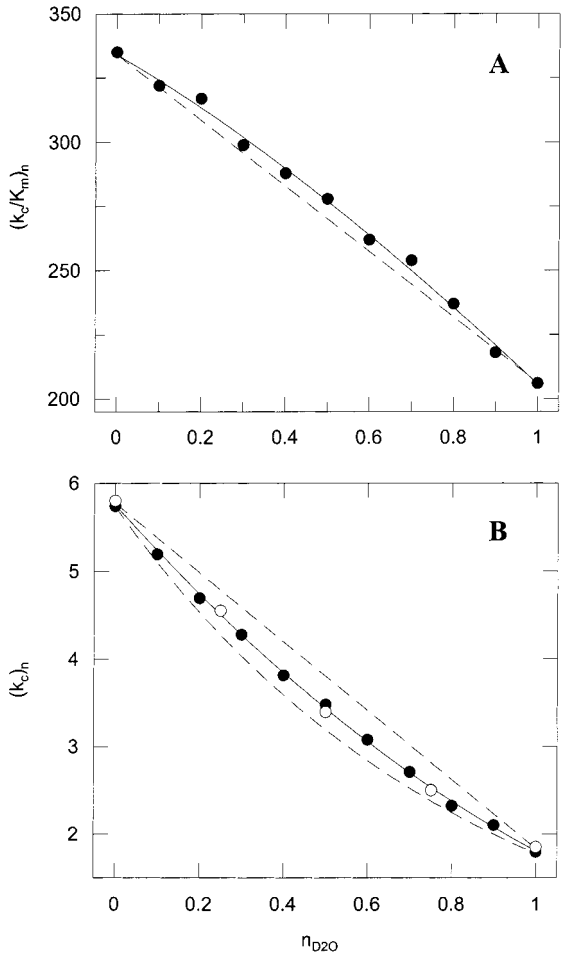

FIGURE 3: Proton inventory for the aryl acylamidase catalyzed hydrolysis of *p*-nitroacetanilide. (Panel A) Values of $(k_c/K_m)_n$, determined from first-order progress curves at low substrate concentration ([PNAA] = 2.0 μM ≤ $0.08K_m$; [AAA] = 70 nM; 25 °C), are plotted here as a function of the mole fraction solvent deuterium, n_{D_2O}, at which they were determined. The solid line through the data was drawn using eq 9 with $i = 1$ and best-fit parameters: $(k_c/K_m)_{n=0} = 334 \pm 2$ mM^{-1} s^{-1}, $Z = 1.21 \pm 0.06$, and $\phi^T = 0.509 \pm 0.028$. For comparison to the experimental data, the straight dashed line was drawn using eq 9 with Z = 1, $i = 1$ and $\phi^T = 0.318$. (Panel B) Steady-state velocities were determined at $[PNAA]_o = 10K_m$, divided by enzyme concentration to yield values of $(k_c)_n$, and plotted here as a function of n_{D_2O}. The filled and empty circles represent two independent experiments. The solid, bowed-down line through the data was drawn using eq 9 with $Z = 1$ and the best-fit parameters: $(k_c)_{n=0} = 5.76 \pm 0.02$ s^{-1} and $\phi^T = 0.662 \pm 0.037$, and $i = 2.8 \pm 0.4$. For comparison, the straight dashed line was drawn with $i = 1$, $\phi^T = 0.318$ (eq 9), while the lower bowed-down dashed line was drawn with $i =$ oo, $\phi^T = 0.31$ (eq 10). Reaction conditions: 50 mM Bicine, 500 mM KCl, pH 10.0, 25 °C. [PNAA] = 250 μM; [AAA] = 18 nM.

A number of mechanisms can give rise to dome-shaped proton inventories (*10*−*12*). In the present case, we favor the simplest mechanism in which isotope-effect-generating solvation changes are accompanied by binding of substrate to the enzyme and then followed by acylation of the active site serine. Such a mechanism would generate a proton inventory that obeys the general expression of eq 9. In this case, Z can be taken to be the solvent isotope effect on K_s (*11, 12*), while $(1/\phi^T)^i$ corresponds to the solvent isotope effect on k_{acyl}. The proton inventory for this sort of mechanism takes on a final shape that is an average of contributions from the Z^n term, which tends toward a dome shape (Z

Table 2: Analysis of the Proton Inventory for k_c/K_m for Aryl Acylamidase-Catalyzed Hydrolysis of *p*-Nitroacetanilide[a]

i	$(k_c/K_m)_{n=0}$ (mM^{-1} s^{-1})	Z	ϕ^T	$(1/\phi^T)^i$	χ^2
1	334 ± 2	1.2 ± 0.1	0.51 ± 0.03	2.0	7.31
2	334 ± 2	1.6 ± 0.1	0.62 ± 0.02	2.6	7.52
3	334 ± 2	2.0 ± 0.1	0.68 ± 0.03	3.2	7.65
4	334 ± 2	2.3 ± 0.3	0.72 ± 0.02	3.8	7.73
5	334 ± 2	2.7 ± 0.3	0.74 ± 0.02	4.4	7.79

[a] The proton inventory of Figure 3A were fit to eq 9 with *i* constrained to the indicated value.

Table 3: β-Deuterium Isotope Effects on k_c/K_m for the Aryl Acylamidase-Catalyzed Hydrolysis of *p*-Nitroacetanilide[a]

experiment[b]	$10^5 k_H$ (s^{-1})	$10^5 k_D$ (s^{-1})	k_H/k_D
1	1269 ± 34	1503 ± 27	0.844 ± 0.027
2	1258 ± 75	1520 ± 48	0.828 ± 0.056

[a] Reaction conditions: 50 mM Bicine, 500 mM KCl, pH 10, 25 °C. [PNAA] = [d_3–PNAA] = 2.0 μM; [AAA] = 70 nM. [b] In each experiment, four to six replicate first-order reaction progress curves were collected for each of the two isotopically labeled compounds.

> 1), and by the $(1 - n + n\phi^T)^i$ term, which tends toward either linearity ($\phi^T < 1$, $i = 1$) or bowl-shape ($\phi^T < 1$, $i > 1$). Now, attempts at fitting the data of Figure 3A to eq 9 resulted in nonconvergence, due to the interdependence of the parameters, but if we first constrained *i*, the fits converged as summarized in Table 2. We see that as *i* increases, resulting in a deeper bowl, *Z* must also increase to maintain a fit to the data. The fits to the data become less good, as judged by χ^2 values, but only slightly so. Thus, there is no unique fit to the data and other criteria will have to be used to decide which of these mechanisms best describes the data.

The proton inventory data for k_c (Figure 3B) generates an overall isotope effect of 3.16 that is in good agree with the $^{D_2O}k_c$ value of 3.5 reported above. In contrast to the proton inventory for k_c/K_m, this proton inventory is bowl-shaped, suggesting that *Z* must be near unity and that the number of protons that are "in-flight" in the transition state for k_c must be greater than 1 (*10*). Fitting the data of Figure 3B to eq 9 provides the following: $(k_c)_{n=0} = 5.76 \pm 0.02$ s^{-1}, $Z = 0.9 \pm 0.3$, $\phi^T = 0.63 \pm 0.09$, and $i = 2.3 \pm 1.2$ ($\chi^2 = 0.0016$). This exercise shows us that *Z* is, in fact, unity. If the data are now refit to eq 9 with *Z* constrained to 1, the following results are obtained: $(k_c)_{n=0} = 5.76 \pm 0.02$ s^{-1}, $\phi^T = 0.662 \pm 0.037$, and $i = 2.8 \pm 0.4$ ($\chi^2 = 0.0013$). Note that the mechanism that is implicit in eq 3 involves a single rate-limiting transition state. We see below that this is an oversimplification and that a more complex mechanism is required.

β-Deuterium Isotope Effects for the Aryl Acylamidase-Catalyzed Hydrolysis of p-Nitroacetanilide. To probe the structure of the rate-limiting transition states for AAA catalysis, we determined the β-deuterium isotope effects for both k_c/K_m and k_c. For k_c/K_m, reaction progress curves were collected at $[S]_o = 2.0\ \mu M = 0.08K_m$ and fit to a first-order rate law to obtain values of $k_{obs} = (k_c/K_m)[E]_o$. Replicate kinetic runs were recorded for each of the two isotopically labeled compounds, PNAA and d_3-PNAA. The mean and standard deviation of k_{obs} calculated from these kinetic runs, together with their ratio (i.e., the isotope effect, k_H/k_D), for two independent experiments are summarized in Table 3.

Table 4: β-Deuterium Isotope Effects on k_c for the Aryl Acylamidase-Catalyzed Hydrolysis of *p*-Nitroacetanilide[a]

experiment[b]	$10^5 v_H$ (OD/min)	$10^5 v_D$ (OD/min)	v_H/v_D
1	3314 ± 34	3426 ± 27	0.967 ± 0.016
2	3216 ± 24	3382 ± 32	0.951 ± 0.011

[c] Reaction conditions: 50 mM Bicine, 500 mM KCl, pH 10, 25 °C. [PNAA] = [d_3–PNAA] = 250 μM; [AAA] = 18 nM. [d] In each experiment, four to six replicate initial velocities were determined for each of the two isotopically labeled compounds.

Scheme 3: Acylenzyme Mechanism for Serine Hydrolases in the Presence of the Exogonesously Added Hydroxylamine Nucleophile

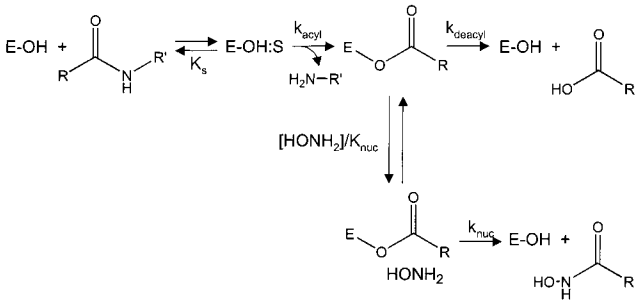

To determine the β-deuterium isotope effect on k_c, steady-state velocities were determined at $[S]_o = 250\ \mu M = 10K_m$. Replicate kinetic runs were recorded for each of the two isotopically labeled compounds, PNAA and d_3-PNAA. The mean and standard deviation of v_{ss} calculated from these kinetic runs, together with their ratio (i.e., v_H/v_D), for two independent experiments is summarized in Table 4.

Aryl Acylamidase-Catalyzed Hydrolysis of p-Nitrophenylacetate. Initial velocities were determined for the AAA-catalyzed hydrolysis of PNPA at six substrate concentrations that ranged from 4 to 125 μM (50 mM Bicine, 500 mM KCl, pH 8.0; $[AAA]_o = 18$ nM) and fit to the Michaelis−Menten equation. The best-fit kinetic parameters are $k_c = 2.0 \pm 0.1$ s^{-1}, $K_m = 18 \pm 2\ \mu M$, and $k_c/K_m = 110 \pm 12$ mM^{-1} s^{-1}. In an accompanying experiment done under the same experimental conditions for the AAA-catalyzed hydrolysis of PNAA: $k_c = 1.9 \pm 0.1$ s^{-1}, $K_m = 12 \pm 3\ \mu M$, and $k_c/K_m = 160 \pm 19$ mM^{-1} s^{-1}. The identity of k_c values for these two substrates suggests rate-limiting deacylation for both reactions.

Effect of Hydroxylamine on k_c for the Aryl Acylamidase-Catalyzed Hydrolysis of p-Nitroacetanilide. To confirm rate-limiting deacylation of k_c for the AAA-catalyzed hydrolysis of the anilide substrate PNAA, the hydroxylamine concentration dependence of k_c was determined. If k_c is rate-limited by deacylation, the acyl-enzyme will accumulate in the steady-state and be susceptible not only to hydrolytic deacylation but also deacylation promoted by other nucleophiles, such as hydroxylamine. This mechanism is illustrated in Scheme 3 and obeys the rate law of eq 11.

$$k_{c,obs} = \frac{k_{acyl}\left(k_{deacyl} + \dfrac{k_{nuc}[HONH_2]}{K_{nuc} + [HONH_2]}\right)}{k_{acyl} + \left(k_{deacyl} + \dfrac{k_{nuc}[HONH_2]}{K_{nuc} + [HONH_2]}\right)} \quad (11)$$

The experimental prediction is that $k_{c,obs}$ will increase with increasing concentration of hydroxylamine.

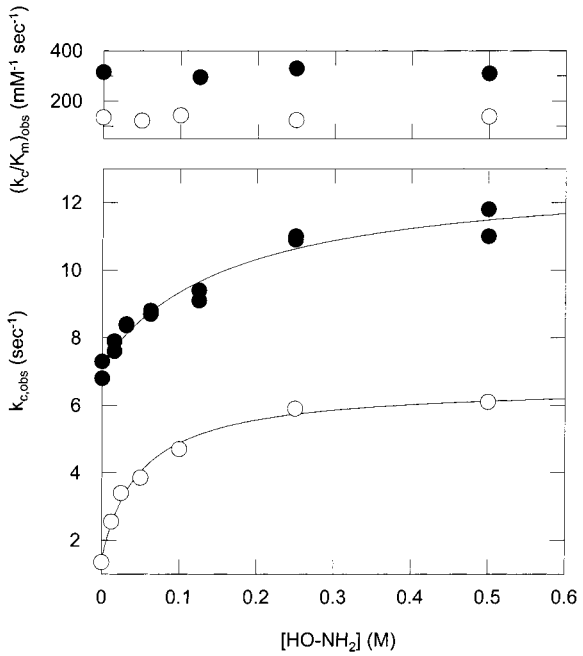

FIGURE 4: Effect of hydroxylamine on k_c and k_c/K_m for the aryl acylamidase-catalyzed hydrolysis of *p*-nitroacetanilide at pH 8.0 (circles) and 10.0 (filled circles). (Lower panel) $k_{c,obs}$ values, determined from steady-state velocities at high substrate concentration ([PNAA] = 250 μM $\geq$ 10K_m; [AAA] = 7 nM; 25 °C), are plotted as a function of hydroxylamine concentration. The solid line was drawn using eq 11 and the best-fit parameters: pH 8.0, $k_{acyl} = 6.6 \pm 0.2$ s^{-1}, $k_{deacyl} = 1.8 \pm 0.3$ s^{-1}, $k_{nuc\_} = 170 \pm 25$ M^{-1} s^{-1}; pH 10.0, $k_{acyl} = 13 \pm 1$ s^{-1}, $k_{deacyl} = 16 \pm 1$ s^{-1}, $k_{deacyl\_} = 180 \pm 50$ M^{-1} s^{-1}. (Upper panel) Values of $(k_c/K_m)_{obs}$, determined from first-order progress curves at low substrate concentration ([PNAA] = 2.0 μM $\leq$ 0.08K_m; [AAA] = 70 nM; 25 °C), were plotted as a function of hydroxylamine concentration. In both cases, hydroxylamine concentration was adjusted by mixing appropriate volumes of the two buffer solutions at the appropriate pH: 50 mM Bicine, 500 mM KCl and 50 mM Bicine, 500 mM potassium hydroxamate.

In these experiments, steady-state velocities were determined at $[S]_o = 250$ μM > 10K_m and found to have a hyperbolic dependence on hydroxylamine concentration (Figure 4, lower panel where $k_{c,obs} = v_{ss}/[E]_o$). Such a dependence can be interpreted in one of two ways: (i) If $K_{nuc} \sim [HONH_2]$, then the observed hyperbolic kinetics results from saturation of the leaving group subsite with hydroxylamine. At low $[HONH_2]$, $k_{c,obs} = k_{acyl}k_{deacyl}/(k_{acyl} + k_{deacyl})$, while at high $[HONH_2]$, $k_{c,obs} = k_{acyl}(k_{deacyl} + k_{nuc})/(k_{acyl} + k_{deacyl} + k_{nuc})$. (ii) If $K_{nuc} \ll [HONH_2]$, then eq 11 simplifies to eq 12

$$k_{c,obs} = \frac{k_{acyl}(k_{deacyl} + k_{nuc}'[HONH_2])}{k_{acyl} + (k_{deacyl} + k_{nuc}'[HONH_2])} \qquad (12)$$

where k_{nuc}' equals k_{nuc}/K_{nuc}, the second-order rate constant for nucleophilic attack on the acyl-enzyme to form acetyl hydroxamate. For this mechanism, hyperbolic kinetics results from a change in the rate-limiting step that is $[HONH_2]$-dependent. At low $[HONH_2]$, $k_{c,obs}$ again equals $k_{acyl}k_{deacyl}/(k_{acyl} + k_{deacyl})$, while at high $[HONH_2]$, $k_{c,obs} = k_{acyl}$. The latter mechanism is favored, since it is unlikely that hydoxylamine could form a stable and catalytically productive complex with the acyl-enzyme of AAA at the site where *p*-nitroaniline binds. This is supported by the absence of $[HONH_2]$-dependent inhibition of k_c/K_m that would occur if hydroxylamine could bind at this site of free enzyme (Figure 4, upper panel).

When the data of Figure 4 were fit to eq 12, the following best fit results were obtained: pH 8.0, $k_{acyl} = 6.6 \pm 0.2$ s^{-1}, $k_{deacyl} = 1.8 \pm 0.3$ s^{-1}, $k_{nuc\_} = 170 \pm 25$ M^{-1} s^{-1}; pH 10.0, $k_{acyl} = 13 \pm 1$ s^{-1}, $k_{deacyl} = 16 \pm 1$ s^{-1}, $k_{deacyl\_} = 180 \pm 50$ M^{-1} s^{-1}. These results indicate that at pH 8, k_c is largely (~80%) determined by deacylation, while at pH 10, k_c is roughly equally rate-limited by acylation and deacylation. The results at pH 8 are consistent with the previous results that, at this pH, k_c values are the same for the AAA-catalyzed hydrolyses of PNPA and PNAA.

Viscosity-Dependence of k_c for the Aryl Acylamidase-Catalyzed Hydrolysis of p-Nitroacetanilide. At $[S]_o = 250$ μM = 10K_m, steady-state velocities were determined as a function of solvent viscosity. The viscogens in these experiments were sucrose and glycerol. While a rate reduction was observed with increasing concentrations of glycerol, none was observed when sucrose was used as the viscogen. Thus, the effect observed with glycerol is some nonspecific inhibition and not a result of a viscosity-dependent k_c.

DISCUSSION

Rate-Limitation of k_c for the Aryl Acylamidase-Catalyzed Hydrolysis of p-Nitroacetanilide. To interpret the pH-dependence and isotope effects for k_c, it is essential to know which reaction step, acylation or deacylation, is rate-limiting. Two methods were used to establish this: (1) comparison of steady-state kinetic parameters for AAA-catalyzed hydrolysis of PNAA and the activated ester PNPA and (2) the dependence of k_c on concentration of hydroxylamine, a nucleophile that can compete with water for the acyl-enzyme.

For the first method, steady-state kinetic parameters determined at pH 8.0 indicated identical values of k_c, suggesting that AAA-catalyzed hydrolysis of both substrates proceeds with rate-limiting deacylation. While rapid acylation is expected for the activated ester PNPA, it conflicts with our chemical intuition for the anilide substrate PNAA, where we expect attack of an alcohol nucleophile (e.g., active site serine) on the carbonyl carbon of an amide to form a ester (e.g., acyl-enzyme) to be slower than subsequent hydrolysis of that ester. Additional support for this unexpected result was sought and was found in the hydroxylamine dependence of k_c for hydrolysis of PNAA.

The results of these experiments indicate that, at pH 8, k_c is largely rate-limited by deacylation, consistent with the above experiment reporting the identity of k_c for the hydrolysis of PNPA and PNAA. Interestingly, at pH 10, k_c is roughly equally rate-limited by acylation and deacylation, suggestive of a pH-dependent change in rate-limiting step for k_c (see below).

Rate-limiting deacylation for the AAA-catalyzed hydrolysis of PNAA finds precedent in catalysis by serine proteases (*13, 14*) and γ-glutamyl transpeptidase (*26*), where k_c has been found to be rate-limited by deacylation during hydrolysis of specific *p*-nitroanilide and amide substrates. In these cases, it was argued that the free energy available from interactions between enzyme and nonreacting portions of the substrate is utilized to stabilize the transition state for acylation, thus allowing this step to proceed faster than the chemically more facile deacylation. These are examples of

Scheme 4: pH Dependence for Aryl Acylamidase Catalysis

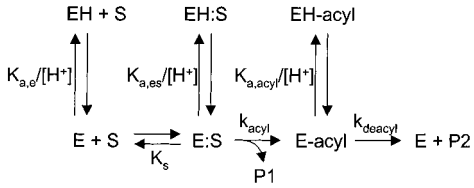

a general strategy for enzymic catalysis which involve the utilization of binding energy derived from remote interactions between enzyme and substrate. This is a principal mechanism for proteases where several orders of magnitude in catalytic enhancement can be gained from interactions between protease subsites and the peptic acyl moiety of the substrate. However, in the present case, the acyl moiety is a simple acetyl group, and there seems to be little opportunity for remote site interactions. Thus, AAA must have other means of paying the energetic price of catalysis.

pH-Dependence of Catalysis by Aryl Acylamidase. The simple pH-dependencies for k_c and k_c/K_m for the AAA-catalyzed hydrolysis of PNAA suggest the single-ionization mechanism of Scheme 4. Equations 13 and 14 describe the pH dependencies for the observed steady-state kinetic parameters in the context of this mechanism:

$$(k_c/K_m)_{obs} = \frac{k_{acyl}/K_s}{1 + \frac{[H^+]}{K_{a,e}}} \tag{13}$$

$$k_{c,obs} = \frac{\frac{k_{acyl}}{\left(1 + \frac{[H^+]}{K_{a,es}}\right)}\frac{k_{deacyl}}{\left(1 + \frac{[H^+]}{K_{a,acyl}}\right)}}{\frac{k_{acyl}}{\left(1 + \frac{[H^+]}{K_{a,es}}\right)} + \frac{k_{deacyl}}{\left(1 + \frac{[H^+]}{K_{a,acyl}}\right)}} \tag{14}$$

The pH dependence of k_c/K_m reveals a single catalytically important ionization of free enzyme governed by a pK_a of 8.15. Given the mechanistic similarity between this enzyme and other serine hydrolases, p$K_{a,e}$ probably corresponds to ionization of an active site His or Lys. However, definitive identification of this residue must await further experimentation. In any event, this result is consistent with the involvement of an ionizable active site residue acting as a general-base catalyst to activate the active site Ser for nucleophilic attack on the carbonyl carbon of the substrate. As discussed below, these results support the conclusions from solvent isotope effects.

The observed pK_a for k_c is 8.54, 0.4 pH units more basic than p$K_{a,e}$. This perturbation in pK_a results from the kinetically complex nature of k_c, which can be fully or partially rate-limited by either k_{acyl} or k_{deacyl}. Examination of eq 14 reveals that, depending upon the values of k_{acyl}, k_{deacyl}, p$K_{a,es}$, and p$K_{a,acyl}$, one can anticipate two phenomena: pH-dependent changes in rate-limiting step and observed values of pK_a that are a weighted average of the two microscopic dissociation constants, p$K_{a,es}$ and p$K_{a,acyl}$. In light of these considerations, it was of some interest to see if the pH dependence of k_c could be fit to eq 14 using reasonable parameter values. Attempts at directly fitting the data of Figure 1B to eq 14 resulted in nonconvergence, but if we constrained p$K_{a,es}$ to a value similar in magnitude to p$K_{a,e}$, and k_{acyl} and k_{deacyl} to their experimentally determined values of 13 and 16 s^{-1}, respectively, an excellent fit to the data of Figure 1B can be obtained with a value of p$K_{a,acyl}$ equal to 8.8. The theoretical line generated in this way is superimposable on the line that is shown in Figure 1B, demonstrating the success of this model in accounting for the experimental data for k_c.

Solvent Deuterium Isotope Effects. The solvent deuterium isotope effects on k_c and k_c/K_m are 3.5 and 1.7, respectively. Interpreted broadly, these results suggest a reaction mechanism for AAA involving rate-limiting chemistry with some form of protolytic catalysis and are consistent with the pH dependencies of k_c and k_c/K_m, which suggest the catalytic involvement of a basic active site residue.

A more detailed analysis of these isotope effects begins with an attempt to understand the large difference in magnitude between $^{D_2O}k_c$ and $^{D_2O}(k_c/K_m)$. We start with an examination of how $^{D_2O}k_c$ and $^{D_2O}(k_c/K_m)$ relate to the solvent isotope effects for the mechanistic parameters of Scheme 2, that is, $^{D_2O}K_s$, $^{D_2O}k_{acyl}$, and $^{D_2O}k_{deacyl}$. These relationships are expressed in eqs 15 and 16.

$$^{D_2O}(k_c/K_m) = {}^{D_2O}(k_{acyl}/K_s) = \frac{^{D_2O}k_{acyl}}{^{D_2O}K_s} \tag{15}$$

$$^{D_2O}k_c = \frac{^{D_2O}k_{acyl}\,{}^{D_2O}k_{deacyl}}{^{D_2O}k_{acyl} + {}^{D_2O}k_{deacyl}} = C_{acyl}\,{}^{D_2O}k_{acyl} + C_{deacyl}\,{}^{D_2O}k_{deacyl} \tag{16}$$

In eq 16, C_{acyl} and C_{deacyl} are coefficients that reflect relative contributions to rate-limitation by k_{acyl} and k_{deacyl}, respectively, and are defined in eqs 17 and 18 (*3*).

$$C_{acyl} = \frac{k_c}{k_{acyl}} = \left(1 + \frac{k_{acyl}}{k_{deacyl}}\right)^{-1} \tag{17}$$

$$C_{deacyl} = \frac{k_c}{k_{deacyl}} = \left(1 + \frac{k_{deacyl}}{k_{acyl}}\right)^{-1} \tag{18}$$

Recall from the experiments in which we examined the hydroxylamine-promoted partitioning of the acyl-enzyme that, at pH 10, k_c, k_{acyl}, and k_{deacyl} are 7.2, 13, 16 s^{-1}, respectively. These values together with eqs 17 and 18 allow us to calculate values of C_{acyl} and C_{deacyl} equal to 0.55 and 0.45, respectively.

We can now examine the dependence of $^{D_2O}k_{acyl}$ and $^{D_2O}k_{deacyl}$ on $^{D_2O}K_s$ using eqs 15 and 16 together and the calculated values of C_{acyl} and C_{deacyl}. These dependencies are shown in Figure 5, where we see that as $^{D_2O}K_s$ increases over the common range for this parameter of from 1 to 2 (*11*,-*12*), $^{D_2O}k_{acyl}$ increases linearly from 1.7 to 3.3, while $^{D_2O}k_{deacyl}$ decreases linearly from 5.7 to 3.6. Thus, to account for the difference in solvent isotope effects for k_c and k_c/K_m, $^{D_2O}k_{acyl}$ must be significantly less than $^{D_2O}k_{deacyl}$.

This range of $^{D_2O}K_s$ values, as well as the calculated values of $^{D_2O}k_{acyl}$ shown in Figure 5, are consistent with our analysis of the proton inventory for k_c/K_m. Recall that for the cases

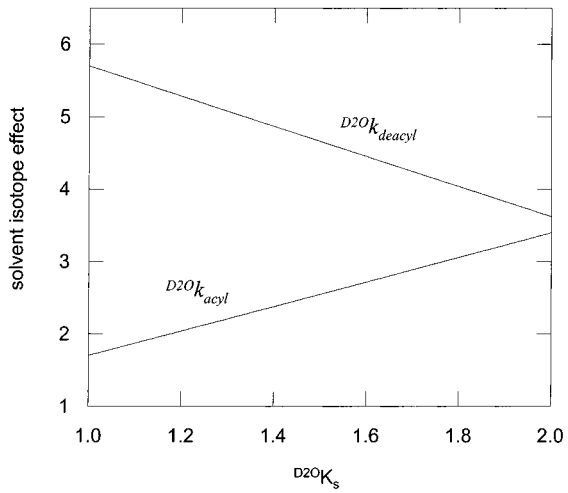

FIGURE 5: Dependence of solvent isotope effects for acylation and deacylation on $^{D_2O}K_s$. The dependence of $^{\beta D}k_{acyl}$ and $^{\beta D}k_{deacyl}$ on $^{D_2O}K_s$ was calculated using eqs 15−18. See text for details.

of one or two transition state protons in flight, we determined $^{D_2O}K_s$ values (equivalent to *Z*) of 1.2 or 1.6, respectively, and $^{D_2O}k_{acyl}$ values of 2.0 or 2.6, respectively (see Table 2). Thus, the acylation process, as governed by k_c/K_m, generates isotope effects on mechanistic parameters (i.e., *i*, $^{D_2O}K_s$, and $^{D_2O}k_{acyl}$) whose magnitudes are well within the common range for serine hydrolases. The most conservative view is that PNAA binds to AAA by a process that generates a small solvent isotope effect of solvation of about 1.2 and then acylates the active site serine with simple general-base catalysis that generates an isotope effect of 2 resulting from a single transition state proton in flight.

Now, if $^{D_2O}k_{acyl}$ is 2.0, we can use eq 16 to calculate a $^{D_2O}k_{deacyl}$ value of 5.3. While this latter value may seem unusually large, it does find precedent in the solvent isotope effect of 4.3 on k_c that was observed for the trypsin-catalyzed hydrolysis of Bz-Phe-Val-Arg-pNA (*15*), the solvent isotope effect of 4.7 on the conformational isomerization of ribonuclease A (*16*), and the solvent isotope effect of 4.9 on product release for cAMP-dependent protein kinase (*17*).

To help interpret $^{D_2O}k_{deacyl}$, we will further analyze the proton inventory for k_c. Recall that the proton inventory of k_c is bowl-shaped (see Figure 3B) and indicates that two or more protons are "in flight" in the rate-limiting transition state for k_c. This simple analysis is, of course, inadequate, since we now know that k_c is a composite of contributions to rate-limitation from both acylation and deacylation.

A more complete analysis of the proton inventory for k_c begins with eq 19

$$k_{c,n} = \left\{ \frac{1}{k_{acyl}(1 - n + n\phi^{T,acyl})^i} + \frac{1}{k_{deacyl}(1 - n + n\phi^{T,deacyl})^j} \right\}^{-1} \quad (19)$$

where the terms take their meaning as outlined in the Results. In this analysis, values for k_{acyl} and k_{deacyl} can be calculated to be 10.4 and 12.8 s^{-1}, respectively, from the observed $k_{c,0}$ value of 5.74 s^{-1}, the C_{acyl} and C_{deacyl} values of 0.55 and 0.45, and eqs 17 and 18. The fractionation factors can be calculated in the following way. Given an overall solvent isotope effect of 3.2 for this experiment and assuming a solvent isotope effect of 1.2 on K_s (see above), we can calculate values of $^{D_2O}k_{acyl}$ and $^{D_2O}k_{deacyl}$ of 2.0 and 5.3, respectively. These values can then be used to set the following constrains to eq 19: $(\phi^{T,acyl})^i = 2.0^{-1}$ and $(\phi^{T,deacyl})^j = 5.3^{-1}$. What this means is that regardless of the number of protonic sites that contribute to the isotope effects for acylation and deacylation, $^{D_2O}k_{acyl}$ must equal 2.0 and $^{D_2O}k_{deacyl}$ must equal 5.3.

With the above values in hand, this analysis reveals the following: when *i* and $\phi^{T,acyl}$ are constrained to 1 and 0.50, respectively, $j = 11 \pm 2$ and $\phi^{T,deacyl} = 0.87 \pm 0.02$ ($\chi^2 = 0.0014$), and when *i* and $\phi^{T,acyl}$ are constrained to 2 and 0.71, respectively, $j = 6 \pm 1$ and $\phi^{T,deacyl} = 0.78 \pm 0.03$ ($\chi^2 = 0.0014$). Values of *i* larger than 2 produce increasingly poorer fits to the data. Thus, it appears that acylation proceeds through a transition state in which one or two protons are in flight, while in the transition state for deacylation, no fewer than five protons are in flight. Further interpretation of these results to provide a transition state structure for k_{acyl} and k_{deacyl} must await a discussion of the β-deuterium isotope effects.

β-Deuterium Isotope Effects. To further probe the structure of the rate-limiting transition(s) states for the AAA-catalyzed hydrolysis of PNPA, β-deuterium isotope effects were determined. In acyl-transfer reactions proceeding either by a two-step mechanism through a tetrahedral intermediate or by a one-step mechanism with a quasi-tetrahedral transition state, deuterium substitution on the carbon adjacent to the carbonyl ("β-D" substitution) is expected to increase the rate (*18*). This is because, in the partially tetrahedral transition state (whether before, after, or instead of the tetrahedral intermediate), hyperconjugation from the β-CH(D) bonds is reduced, increasing the electron density in the bonds and strengthening them (thus giving an inverse isotope effect). In the present case, rate constant measurements for the AAA-catalyzed hydrolysis of PNPA and d_3-PNPA generated the following isotope effects: $^{\beta D}(k_c/K_m) = 0.83 \pm 0.04$ and $^{\beta D}k_c = 0.96 \pm 0.01$.

The isotope effects on the microscopic rate constant, $^{\beta D}k_{acyl}$ and $^{\beta D}k_{deacyl}$, can be calculated using these values of $^{\beta D}(k_c/K_m)$ and $^{\beta D}k_c$, expressions analogous to eqs 15 and 16, C_{acyl} and C_{deacyl} values of 0.55 and 0.45, respectively, and some assigned value for $^{\beta D}K_s$. Unfortunately, it is not at all clear what value to assign $^{\beta D}K_s$. Isotope effects for the partitioning of PNAA from cyclohexane to water (*19*) suggest that $^{\beta D}K_s$ is inverse and could be as small as 0.94 if Michaelis complex inteactions are primarily hydrophobic relative to solvated substrate. On the other hand, gas-phase calculations comparing acetaldehyde, $L_3C(C{=}O){-}H$, and protonated acetaldehyde, $L_3C(C{=}OH^+){-}H$ (L = H, D) (*20*) suggest normal values as large as 1.3 for $^{\beta D}K_s$ if Michaelis complex interactions polarize the carbonyl. In these calculations, I took a conservative view, assumed importance for both substrate desovlation and polarizing active site interactions, and assigned a value of unity to $^{\beta D}K_s$. The following can now be calculated: $^{\beta D}k_{acyl} = 0.83$ and $^{\beta D}k_{deacyl} = 1.12$.

Transition State Structures for k_{acyl} and k_{deacyl}. The combination of pH dependencies, solvent deuterium isotope effects, and β-deuterium isotope effects allows us to formulate the following transition state structures for the reaction steps governed by k_{acyl} and k_{deacyl}.

Scheme 5: Map of Alternate Routes for Decomposition of the Tetrahedral Intermediate Formed during Acylation of Aryl Acylamidase by *p*-Nitroacetanilide

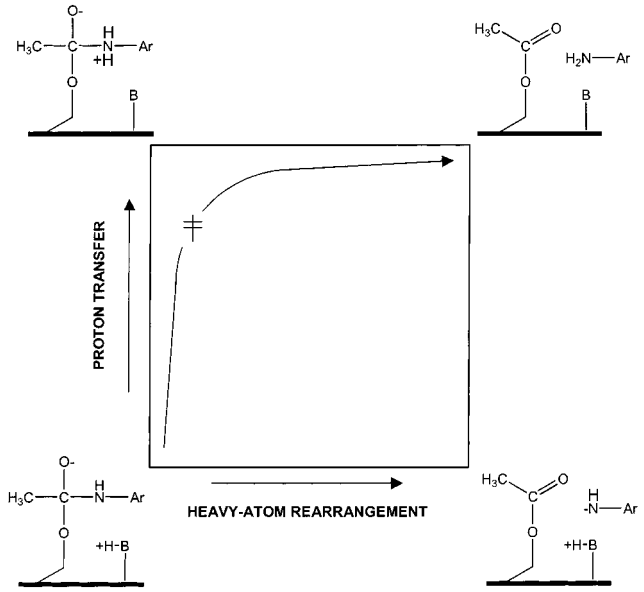

The isotope effect data suggests that k_{acyl} is rate-limited entirely by the chemistry of serine acylation. Given a solvent isotope effect that lies between 2.0 and 2.6, this reaction is general-base catalyzed and, based on the proton inventory analysis, involves transfer of one or two catalytically important protons. The large β-deuterium isotope on k_{acyl} of 0.83 suggests that the transition state for k_{acyl} has substantial tetrahedral character. Now, in the alkaline hydrolysis of *p*-nitroacetanilide at low hydroxide concentration, the rate-limiting step is expulsion of the *p*-nitroaniline leaving group from the tetrahedral intermediate (*3, 18*). It is not unreasonable to suppose that the same situation might apply to the enzymatic hydrolysis of *p*-nitroacetanilide. If this were the case, then the substrate-derived portion of the activated complex for k_{acyl} must bear very close structural analogy to the tetrahedral intermediate that precedes it on the reaction pathway, and thus, these isotope effects indicate that proton transfer is well-advanced of heavy atom rearrangement in the transition state. This is illustrated in the MARS diagram of Scheme 5, where the position of the transition state for acylation, as deduced from the isotope effects, is shown on the reaction coordinate, which comprises elements of heavy-atom rearrangement and proton transfer. In this transition state, proton transfer from the protonated base to the departing aniline nitrogen is nearly compete with relatively little rehybridization at the tetrahedral carbon of the addition adduct and, implicitly, relatively little C−N bond fission.

The situation for k_{deacyl} is not so simple. The large solvent isotope effect of 5 is generated from hydrogen fractionation at no less than five protonic sites and is suggestive of a conformational isomerization of the enzyme. The large, normal β-deuterium isotope effect of 1.12 indicates an *increase* in hyperconjugation in the β-CH(D) bonds as the transition state for k_{deacyl} is entered. These are unusual isotope effects and, thus, eliminate many simple mechanisms for deacylation. However, an attractive mechanism that can account for these results is one in which a rate-limiting conformational change of the acyl-enzyme repositions the acetyl moiety so that the carbonyl bond is in an environment that polarizes it. This would facilitate nucleophilic attack of water as well as generate a normal β-deuterium isotope effect. Furthermore, if the conformational change was coupled to multiple protonic sites, such a mechanism could also generate a large solvent isotope effect.

The absence of a viscosity effect on k_c indicates that if this mechanism obtains, the proposed conformational change is not global but rather localized to the active site. A global, rate-limiting conformational isomerization of the acyl-enzyme would be anticipated to produce k_c values that decrease with increasing solvent viscosity (*21, 22*), even for a case where k_c is only partially rate-limited by deacylation.

Catalysis by Aryl Acylamidase. A principal goal of enzymology is to understand the molecular origins of enzyme catalytic power. In the context of transition state rate theory, catalysis occurs when specific, stabilizing interactions are formed between substrate and catalyst in the activated complex for the catalyzed reaction that do not exist in the activated complex for the uncatalyzed reaction. Thus, the transition state for the catalyzed reaction has a free energy that is smaller in magnitude than the free energy of the uncatalyzed reaction, relative to the common ground state for the uncatalyzed and catalyzed reactions. The energy difference between the two transition states can be refereed to as ΔG^*_{cat}. To understand the molecular origins of ΔG^*_{cat} for enzymic reactions, and thus the molecular origins of enzyme catalysis, we will require detailed structures for the following species: (1) substrate and the enzyme in their ground state, (2) activated complex of the uncatalyzed reaction, and (3) activated complex of the catalyzed reaction. If sufficiently detailed, these structures can serve as a basis for energetics calculations that will allow a dissection of the ΔG^*_{cat} value into specific interactions between enzyme and substrate. Such a strategy for investigating enzymic catalytic power was suggested by Schowen and co-workers nearly 25 years ago (*23, 24*). Schowen explains that

> The free energy liberated by the binding of the standard reaction transition state to the enzyme is calculable from experimental data, being the difference between the free energies of activation for the catalyzed and uncatalyzed reactions, and is thus called the *empirical free energy of binding of the transition state* [i.e., ΔG^*_{cat}]. This empirical binding energy can usefully be separated conceptually into two additive terms: *the free energy of distortion* for distorting the free enzyme and the standard-reaction transition state into the forms they will have in the enzymic transition state ("poised structures") and *the vertical free energy of binding* for bringing the poised structures together from their standard-state distributions and forming the enzymic transition state by their interaction. This suggests a program of investigation of enyzmic catalytic power involving (1) determination of standard-reaction and enzymic transition-state structures, (2) investigation of the energy requirements for distortion to the poised structures, and (3) investigation of the free- energy associated with combination of the poised structures (*25*).

In the present study, we found that the second-order rate constant k_E ($=k_{acyl}/K_s$) for reaction of *p*-nitroacetanilide with aryl acylamidase is 3.4×10^5 M^{-1} s^{-1}. This rate constant reflects the energy difference between the reactant state of enzyme and substrate free in solution and the rate-limiting transition state for acylation (see Scheme 5), which likely

Scheme 6: Analysis of Catalytic Efficiency for Aryl Acylamidase[a]

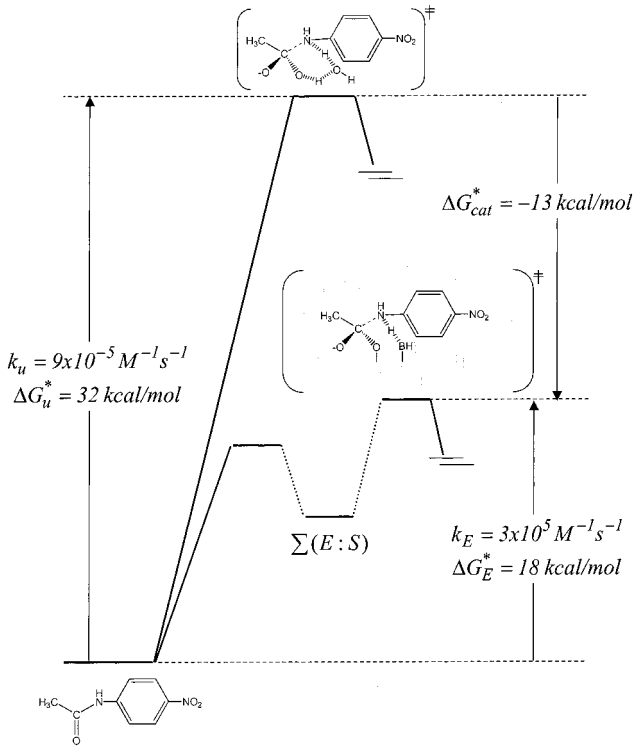

[a] In the calculation of free energy values, standard-state enzyme and hydroxide concentrations were set at 10^{-6} M, and temperature was set to 298 °C

corresponds to expulsion of the *p*-nitroaniline leaving group from the tetrahedral intermediate to produce the acyl-enzyme. To assess the catalytic enhancement that this enzyme brings about, we need to compare this reaction and rate constant to a nonenzymatic hydrolytic reaction of *p*-nitroacetanilide. An appropriate standard is the alkaline hydrolysis of *p*-nitroacetanilide at low hydroxide concentration. This reaction is governed by the second order-rate constant k_2 ($=k_2\_k_1/k_{-1}$, see Scheme 1), which equals 9×10^{-5} M^{-1} s^{-1} (*3*). k_2 reflects the energy difference between the reactant state of hydroxide and substrate and the rate-limiting transition of decomposition of the tetrahedral intermediate (*4*). The clear chemical analogy between the reactions governed by k_E and k_2 allows mechanistic interpretation of the ratio k_E/k_2. This catalytic enhancement ratio of 3×10^9 corresponds to a ΔG^*_{cat} of 13 kcal/mol and reflects the stabilizing interactions that exist in the activated complex of the enzymatic reaction but do not exist in the hydroxide reaction (see Scheme 6).

At this point, our information concerning the origin of ΔG^*_{cat} is rudimentary and pertains chiefly to the substrate-derived portion of the activated complex for the uncatalyzed and catalyzed reactions. For the standard reaction, $^{\beta D}k_2$ is 0.90 ± 0.02 (*3*) and suggests substantial tetrahedral character but less relative to enzymic reaction where $^{\beta D}k_E$ is 0.83 ± 0.04. We also know that in both the enzymic and standard reaction, protolytic assistance of *p*-nitroaniline expulsion is important. In the hydroxide reaction, protolytic assistance is from solvent (*4*). What is, of course, missing is any structural information about either the enzyme in the activated complex or solvent reorganization. The former is essential for the assessment of the *free energy of distortion*, while the latter for the *vertical free energy of binding*. This information can, in principle, be obtained from a combination of kinetic and computational studies (*24*).

We see then that concepts of transition state rate theory are expected to be sufficient to explain enzymatic hydrolysis of *p*-nitroacetanilide and, indeed, enzyme-catalyzed reactions in general. While answering questions concerning protein dynamics is clearly critical to a complete understanding of enzymatic reactions, these answers may be irrelevant to the very specific task of explaining how enzymes bring about their catalytic enhancements since, by definition, catalysis is a two state problem independent of reaction path.

REFERENCES

1. Radzicka, A., and Wolfenden, R. (1996) *J. Am. Chem. Soc. 118*, 6105−6109.
2. Brown, R. S., Bennett, A. J., and Slebocka-Tilk, H. (1992) *Acc. Chem. Res. 25*, 481−488.
3. Stein, R. L. (1981) *J. Org. Chem. 46*, 3328−3330.
4. Stein, R. L., Fujihara, H., Quinn, D. M., Fischer, G., Kuellertz, G., Barth, A., and Schowen, R. L. (1984) *J. Am. Chem. Soc. 106*, 1457−1461.
5. Young, J. K., Pazhanisamy, S., and Schowen, R. L. (1984) *J. Org. Chem. 49*, 4148−4152.
6. Pollack, R. M., and Dumsha, T. C. (1974) *FEBS Lett. 38*, 292−294.
7. Heymann, E., and Rix, H. (1978) *Int. J. Pept. Protein Res. 11*, 5964.
8. Hammond, P. M., Price, C. P., and Scawen, M. D. (1983) *Eur. J. Biochem. 132*, 651−655.
9. Stein, R. L. (1983) *J. Am. Chem. Soc. 105*, 5111−5116.
10. Quinn, D. M., Sutton, L. D. (1991) In *Enzyme Mechanism from Isotope Effects* (Cook, P. F., Ed.) pp 73−126, CRC Press, Boston.
11. Stein, R. L. (1985) *J. Am. Chem. Soc. 107*, 6039−6042.
12. Stein, R. L., Strimpler, A. M., Hori, H., and Powers, J. C. (1987) *Biochemistry 26*, 1305−14.
13. Rahfeld, J., Schutkowski, M., Faust, J., Neubert, K., Barth, A., and Heins, J. (1991) *Biol. Chem. Hoppe-Seyler 372*, 313−318.
14. Stein, R. L., Viscarello, B. R., and Wildonger, R. A. (1984) *J. Am. Chem. Soc. 106*, 796−798.
15. Elrod, J. P., Hogg, J., Quinn, D. M., Venkatasubban, K. S., and Schowen, R. L. (1980) *J. Am. Chem. Soc. 102*, 3917−3922.
16. Wang, M. S., Gandour, R. D., Rodgers, J., Haslam, J. L., and Schowen, R. L. (1975) *Bioorg. Chem. 4*, 392−406.
17. Zhou, J., and Adams, J. A. (1997) *Biochemistry 36*, 2977−2984.
18. Stein, R. L., Fujihara, H., Quinn, D. M., Fischer, G., Kullertz, G., Barth, A., and Schowen, R. L. (1984) *J. Am. Chem. Soc. 106*, 1457−1461.
19. Kovach, I. M., and Quinn, D. M. (1983) *J. Am. Chem. Soc. 105*, 1947−1950.
20. Hess, R. A., Hengge, A. C., and Cleland, W. W. (1998) *J. Am. Chem. Soc 120*, 2703−2709.
21. Somogyi, B., Welch, G. R., and Damjanovich, S. (1984) *Biochim. Biophys. Acta 768*, 81−112.
22. Ng, K., and Rosenberg, A. (1991) *Biophys. Chem. 41*, 289−299.
23. Schowen, R. L. (1978) In *Transition States of Biochemical Processes* (Gandour, R. D., Schowen, R. L., Eds.) pp 77−114, Plenum Press, New York.
24. Maggiora, G. M., and Schowen, R. L. (1977) In *Bioorganic Chemistry* (van Tamelen, E. E., Ed.) Vol. 1, Acedemic Press, New York.
25. Schowen, R. L. (1978) In Transition States of Biochemical Processes (Gandour, R. D., Schowen, R. L., Eds.) p 112, Plenum Press: New York.
26. Stein, R. L., DeCicco, C., Nelson, D., and Thomas, B. (2001) *Biochemistry 40*, 5804−5811.

BI0118198